International Journal of Solids and Structures 47 (2010) 1592–1602

Contents lists available at ScienceDirect

International Journal of Solids and Structures

journal homepage: www.elsevier.com/locate/ijsolstr

Cyclic thermo-viscoplasticity of high density polyethylene

A.D. Drozdov *

Danish Technological Institute, Gregersensvej 1, DK–2630 Taastrup, Denmark

ARTICLE INFO

Article history:
Received 2 September 2009
Received in revised form 15 February 2010
Available online 3 March 2010

Keywords:
High density polyethylene
Viscoplasticity
Thermal effects
Cyclic deformation

ABSTRACT

Observations are reported in uniaxial cyclic tensile tests (loading–unloading with various maximum strains) on high density polyethylene at temperatures ranging from room temperature up to 90 °C. It is demonstrated that the maximum stress per cycle and an apparent residual strain (measured at the instant when the tensile force vanishes under retraction) strongly decrease with temperature. The latter seems unexpected as the interval of temperatures covers the α-relaxation temperature, which is conventionally associated with activation of additional mechanisms for inelastic flow. A model is developed that captures the decrease in residual strain with temperature. Adjustable parameters in the stress–strain relations are found by fitting the experimental data. The effects of temperature and maximum strain per cycle on residual strains are studied numerically.

1. Introduction

This paper deals with experimental investigation and numerical simulation of the viscoplastic behavior of high density polyethylene (HDPE) in an interval of temperatures covering the α-relaxation region.

Observations in small-amplitude oscillatory tests on polyethylene demonstrate three noticeable peaks on the diagram of loss tangent δ plotted versus temperature T (Popli et al., 1984; Boyd, 1985; Khanna et al., 1985; Alberola et al., 1990). A peak with the highest temperature T_α (located below the melting temperature T_m) is conventionally associated with α-relaxation. For high density polyethylenes, T_α belongs to the interval between 50 and 70 °C (Na et al., 2007). Its position is weakly affected by molecular structure (molecular weight distribution, entanglement density, degree of branching, lamellar thickness, average size of spherulites, etc.) and testing conditions (frequency of oscillations, heating rate, intensity of preloading, etc.). For recent DMTA (dynamic mechanical thermal analysis) observations on polyethylenes, see Matthews et al. (1999), Kuwabara et al. (2000), Mano (2001), Sirotkin and Brooks (2001), Matsuo et al. (2003), Men et al. (2003), Kolesov et al. (2005), Stadler et al. (2005), Na et al. (2007), Guan and Phillips (2007), and the references therein.

Although α-relaxation in polyolefins is commonly attributed to thermal activation of some sliding processes at the micro-level (these processes are presumed to be restrained below T_α), the physics behind this phenomenon remains a subject of debate for it is not clear (i) what type of sliding starts at T_α, (ii) in which phase (crystalline or amorphous), and (iii) at which length scale. Several hypotheses have been suggested regarding molecular mechanisms of α-relaxation: *c*-shear within crystalline lamellae (homogeneous shear of crystal blocks in the direction of their *c*-axis) (Sirotkin and Brooks, 2001; Guan and Phillips, 2007), inter-lamellar shear (slip of crystalline blocks past each other) (Matthews et al., 1999; Jiang et al., 2009), sliding of tie molecules and motion of chain folds and loops through crystals (Khanna et al., 1985), diffusion of chains (Men et al., 2003) and defects (Alberola et al., 1990) in crystallites, growth of mobility of chains in the interphase (transition regions located in the close vicinity of lamellar surfaces) (Rastogi et al., 2007), weakening of lamellar coupling and enhancement of segment exchange between crystalline and amorphous phases (Kolesov et al., 2005; Na et al., 2007; Zubova et al., 2007).

Not focusing on a detailed description of these mechanisms, one can conclude that heating of a sample through the α-relaxation region activates motion of chains both in crystalline and amorphous phases due to release of constraints hindering their mobility below T_α (Khanna et al., 1985). It seems plausible to presume that enhancement of molecular mobility may be reflected in mechanical tests as a decrease in elastic moduli (driven by rearrangement of chains), as well as intensification of plastic flow (associated with intra- and inter-lamellar slip) with temperature. The aim of this study is to validate this hypothesis by (i) measuring stress–strain diagrams in cyclic tensile tests at various temperatures T, and (ii) applying the experimental data to evaluate the effect of temperature on Young's moduli of crystalline and amorphous regions.

Although the problem of identification of elastic moduli of amorphous and crystalline phases in a semicrystalline polymer has been formulated a long ago (Boyd, 1979), it has not been satisfactory resolved until now. This may be explained by the fact that

* Tel.: +45 72 20 31 42; fax: +45 72 20 31 12.
E-mail address: Aleksey.Drozdov@teknologisk.dk

0020-7683/$ - see front matter © 2010 Elsevier Ltd. All rights reserved.
doi:10.1016/j.ijsolstr.2010.02.021

the stress–strain diagrams of polyethylene under uniaxial stretching are rather simple to be adequately approximated within a one-phase constitutive model (Drozdov and Christiansen, 2008). As modeling of a semicrystalline polymer as a two-phase composite leads to a noticeable growth in the number of material constants, observations in additional tests are to be employed to ensure an acceptable accuracy in their determination. An attempt to apply experimental data in relaxation tests for this purpose was undertaken by Djokovic et al. (2000). However, their treatment of observations (matching of relaxation curves by a sum of two exponential functions that are presumed to describe the time-dependent response of amorphous and crystalline regions separately) may be questioned. It appears that determination of adjustable parameters in a two-phase model by matching stress–strain diagrams under stretching and retraction may be a more adequate approach as it allows not only elastic moduli, but also plastic strains to be assessed.

Our observations in uniaxial tensile cyclic tests (Section 2) demonstrate that the engineering stress σ strongly decreases with temperature, in accord with the above assumptions. Surprisingly, it is found that the plastic strain evaluated by means of an apparent residual strain (the strain measured when the tensile load vanishes at retraction) decreases with temperature (in contradiction to what is expected based on the concept of temperature-induced activation of molecular mobility). The reduction in residual strain is modest when the maximum strain per cycle ϵ_{max} is lower that the yield strain ϵ_y, and it becomes substantial when ϵ_{max} belongs to the post-yield region of deformations.

The objective of this study is threefold: (i) to report observations on HDPE in tensile cyclic tests with various maximum strains in an interval of temperatures that covers the α-relaxation region, (ii) to derive stress–strain relations for the thermo-viscoplastic response of semicrystalline polymers and to find adjustable parameters by fitting the experimental data, and (iii) to apply these equations to the numerical analysis of the effects of temperature and maximum strain per cycle on residual strains [the importance of these effects for engineering applications was discussed by Olasz and Gudmundson (2005)].

Constitutive models for the viscoelastic and viscoplastic responses of semicrystalline polymers under non-monotonic deformation may be divided into two groups. In models belonging to the first group, a homogenization method is applied that allows a semicrystalline polymer with a complicated micro-structure to be replaced with an equivalent one-phase continuum (Bergstrom et al., 2002; Khan and Krempl, 2006; Drozdov and Christiansen, 2007a,b, 2008; Yakimets et al., 2007; Mizuno and Sanomura, 2009; Sweeney et al., 2009). As the number of adjustable parameters necessary to describe the mechanical behavior of a one-phase medium is relatively small, these parameters can be found with high accuracy by matching observations in conventional tests. A shortcoming of these models is that the influence of external factors (e.g., temperature, humidity, etc.) on mechanical properties of crystalline and amorphous phases cannot be evaluated separately.

Models of the other group treat a semicrystalline polymer as a two-phase composite where crystalline inclusions are distributed in an amorphous matrix (Argon, 1997; Nikolov and Doghri, 2000; Cangemi and Meimon, 2001; van Dommelen et al., 2003, 2007; Nikolov et al., 2006; Bedoui et al., 2006; Ben Hadj Hamouda et al., 2007; Roguet et al., 2007; Brusselle-Dupend and Cangemi, 2008; Diani et al., 2008; Dusunceli and Colak, 2008; Baudet et al., 2009; Regrain et al., 2009). A disadvantage of this approach is that it leads to a noticeable increase in the number of material constants and a pronounced deterioration of accuracy of their determination. To overcome this difficulty, three approaches are employed: (i) ad hoc hypotheses are introduced regarding mechanisms of inelastic deformations [for example, plastic flow is ascribed to the crystalline phase exclusively, while the amorphous phase is treated as merely viscoelastic (Nikolov and Doghri, 2000; Cangemi and Meimon, 2001), or different laws are introduced to characterize plastic deformations in the amorphous and crystalline regions (van Dommelen et al., 2003, 2007)], (ii) observations in mechanical tests are analyzed together with experimental data in other tests [conventionally, small- and wide-angle X-ray diffraction (Argon, 1997; Diani et al., 2008)] that provide information about evolution of the crystalline structure under loading, and (iii) complicated deformation programs are applied for the experimental investigation of the mechanical response [numerical simulation shows that cyclic deformation (Regrain et al., 2009) and tension interrupted by creep (Ben Hadj Hamouda et al., 2007; Roguet et al., 2007; Brusselle-Dupend and Cangemi, 2008) are the programs most sensitive to changes in morphology of semicrystalline polymers].

This study follows the latter approach. High density polyethylene is treated as a two-phase composite, where crystalline inclusions are distributed in an amorphous matrix. Both phases are modeled as viscoplastic media. Appropriate plastic flows are associated with sliding of junctions between chains in the amorphous matrix and intra- and inter-lamellar slips in crystallites. The difference between treatment of plastic deformations in crystalline and amorphous regions consists in the assumption that the strain rate for sliding of junctions in the amorphous matrix is proportional to the deviatoric component of an appropriate stress tensor, whereas the strain rate for slip in crystal blocks equals the sum of strain rates for intra- and inter-lamellar sliding. The former linearly depends on the deviatoric part of the stress tensor in the crystalline phase, and the latter is proportional to the strain rate for macrodeformation.

The exposition is organized as follows. Observations in cyclic tensile tests are reported in Section 2. Stress–strain relations for the thermo-viscoplastic response of a semicrystalline polymer are developed in Section 3. Adjustable parameters are found in Section 4. Some results of numerical simulation are discussed in Section 5. Concluding remarks are formulated in Section 6.

2. Experimental procedure

High density polyethylene Eraclene MM 95 (density 0.953 g/cm^3, melting temperature $T_m = 134\,^\circ$C, melt flow index 4 g/10 min) was purchased from Polimeri Europa (Italy). Dumbbell specimens (ASTM standard D-638) with cross-sectional area 9.8 mm $\times$ 3.8 mm were molded by using injection-molding machine Ferromatic K110/S60-2K.

Mechanical tests were conducted by means of universal testing machine Instron-5568 equipped with a thermal chamber and an electro-mechanical sensor for control of longitudinal strains. The tensile force was measured by a 5 kN load cell. The engineering stress σ was determined as the ratio of axial force to cross-sectional area of specimens in the stress-free state.

Five series of cyclic tensile tests were performed at the temperatures T = 23, 45, 60, 75, and 90 $^\circ$ C. Before measurements started, each specimen was equilibrated at the required temperature T for 30 min. In each test, a sample was stretched with the cross-head speed 20 mm/min (which corresponded to the strain rate $\dot\epsilon = 4 \times 10^{-4}$ s^{-1}) up to a maximum strain ϵ_{max} and retracted with the strain rate $-\dot\epsilon$ down to the zero stress. All series of experiments involved three tests with the maximum strains ϵ_{max} = 0.05, 0.10, and 0.15.

Each test was conducted on a new sample and repeated 3 times to assess reproducibility of measurements. The maximum deviation between engineering stresses measured on different specimens did not exceed 4%.

Observations are reported in Figs. 1–5, where the engineering stress σ is plotted versus tensile strain ϵ (the experimental stress–strain curves present average data over three sets of measurements). These figures show that the stress–strain curves under tension and retraction are (i) nonlinear and (ii) strongly affected by temperature. For example, the maximum stress monitored along loading paths of the stress–strain diagrams decreases approximately by 4 times, from 20.5 MPa at room temperature to 15.2 MPa at $T = 45$, 11.4 MPa at $T = 60$, 8.4 MPa at $T = 75$, and 5.8 MPa at $T = 90\,^\circ$C. An apparent residual strain after a cycle of loading–retraction ϵ_{res} (identified as the strain ϵ measured when the tensile stress σ vanishes at unloading) decreases with temperature T when the maximum strain per cycle ϵ_{max} exceeds the yield strain ϵ_y (corresponding to the point of maximum on the stress–strain curve under stretching). The latter value is close to 0.11, and it is practically independent of temperature. For example, for $\epsilon_{max} = 0.15$, the growth of temperature induced a reduction in residual strain by twice: from 0.079 at room temperature to 0.069 at $T = 45$, 0.061 at $T = 60$, 0.046 at $T = 75$, and 0.039 at $T = 90\,^\circ$C. When the maximum strain per cycle becomes lower than the yield strain, the effect of temperature on residual strain weakens pronouncedly: in tests with $\epsilon_{max} = 0.05$, the strain ϵ_{res} remains practically constant (close to 0.022) at all temperatures below 75 °C and decreases down to 0.015 at $T = 90\,^\circ$C.

In what follows, a semicrystalline polymer is modeled as an incompressible medium. To validate this assumption, additional tensile tests were conducted at room temperature, in which tensile strain ϵ and transverse strain ϵ_t were measured simultaneously by means of longitudinal (model Instron Static 2630-113) and transverse (model Epsilon 3574-250M) extensometers. Stretching of samples was performed with the cross-head speed 20 mm/min. The average (over observations on three specimens) stress–strain diagram $\sigma(\epsilon)$ is depicted in Fig. 1. The characteristic dependence of transverse strain ϵ_t on tensile strain ϵ is reported in Fig. 6, where only data below the yield strain ϵ_y are presented (in this region, no volume growth was observed induced by nucleation, formation, and propagation of micro-voids). Fig. 6 demonstrates that transverse strain ϵ_t increases linearly with ϵ in the intervals of linear elastic response ($0 < \epsilon < 0.015$) and in the sub-yield region $0.015 < \epsilon < 0.1$, but slope of the curve $\epsilon_t(\epsilon)$ suffers an upward jump at $\epsilon \approx 0.015$.

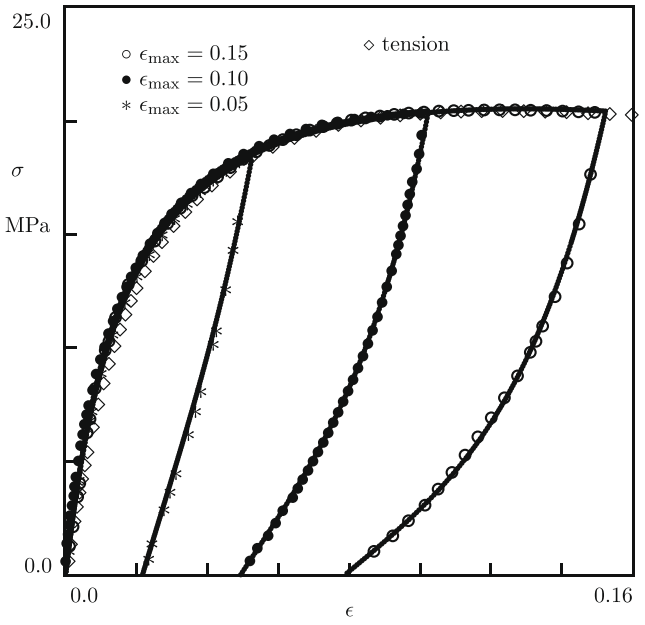

Fig. 1. Stress σ versus strain ϵ. Symbols: experimental data in cyclic tests with various maximum strains ϵ_{max} at $T = 23\,^\circ$C. Solid lines: results of numerical simulation.

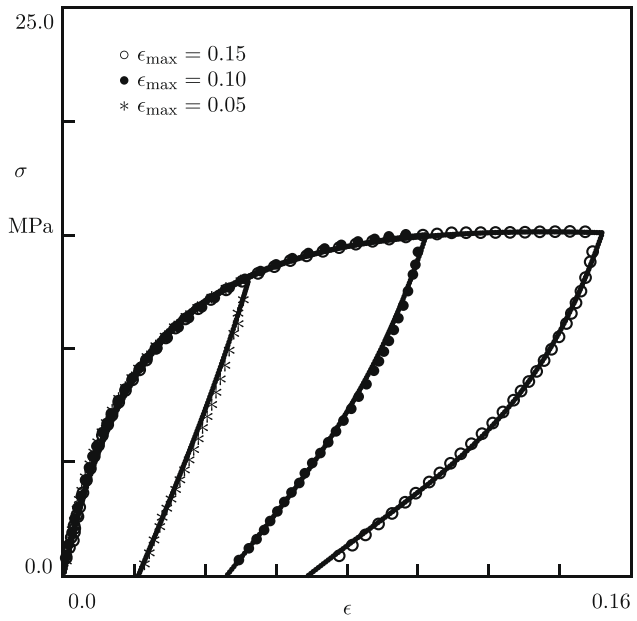

Fig. 2. Stress σ versus strain ϵ. Symbols: experimental data in cyclic tests with various maximum strains ϵ_{max} at $T = 45\,^\circ$C. Solid lines: results of numerical simulation.

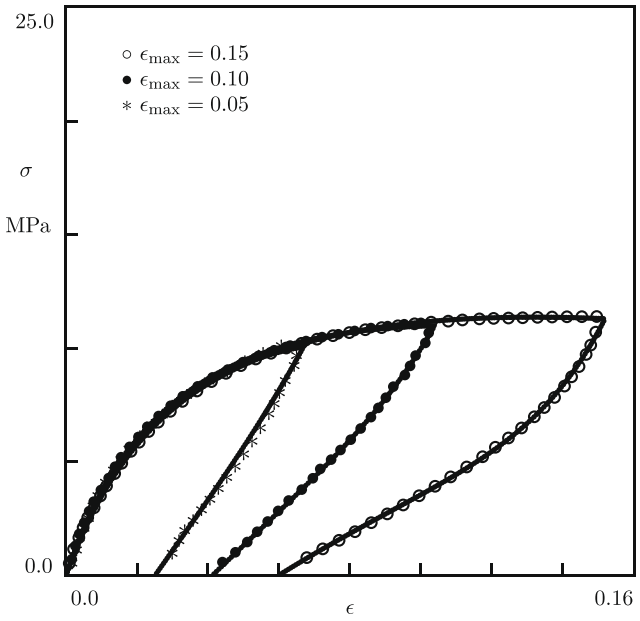

Fig. 3. Stress σ versus strain ϵ. Symbols: experimental data in cyclic tests with various maximum strains ϵ_{max} at $T = 60\,^\circ$C. Solid lines: results of numerical simulation.

To calculate Poisson's ratios of HDPE, the experimental data are approximated by the linear function

$$\epsilon_t = c_0 - c_1\epsilon, \tag{1}$$

where the coefficients c_0 and c_1 are calculated by the least-squares method. Fitting is performed separately in the intervals [0,0.015] and [0.015,0.1], respectively. Poisson's ratios ν_1 (in the region of linear mechanical response) and ν_2 (in the interval of sub-yield deformations) are set equal to appropriate coefficients c_1. Poisson's ratio $\nu_1 = 0.423$ is in good agreement with the values of this param-

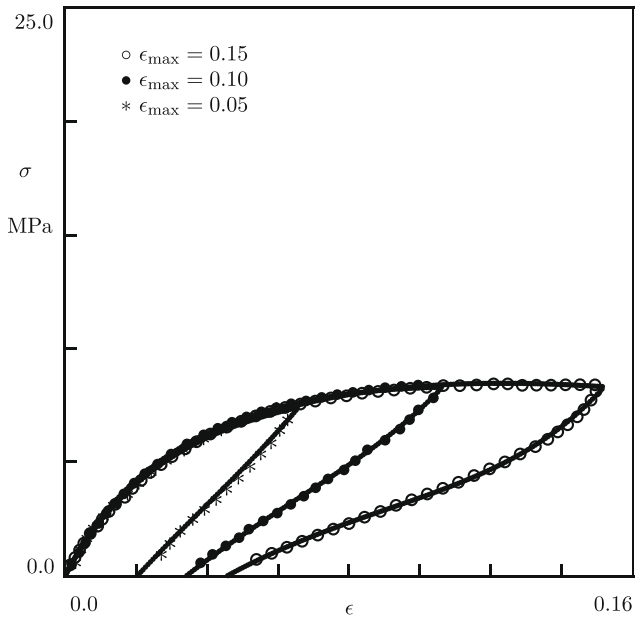

Fig. 4. Stress σ versus strain ϵ. Symbols: experimental data in cyclic tests with various maximum strains ϵ_{max} at $T = 75\,^{\circ}$C. Solid lines: results of numerical simulation.

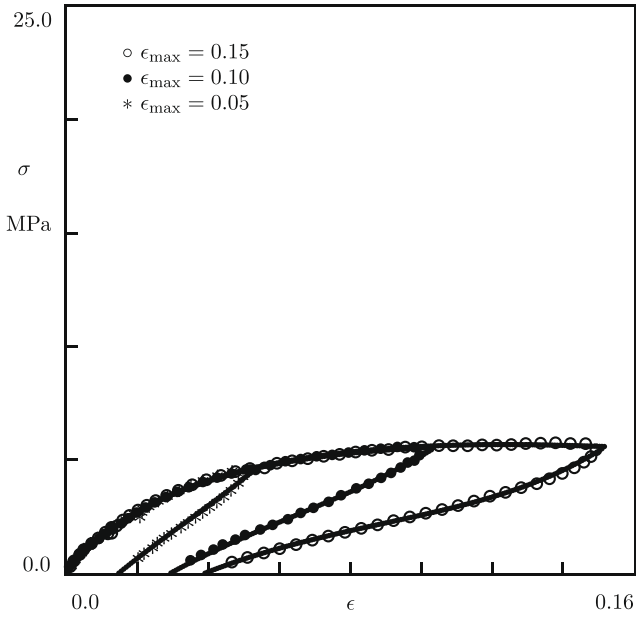

Fig. 5. Stress σ versus strain ϵ. Symbols: experimental data in cyclic tests with various maximum strains ϵ_{max} at $T = 90\,^{\circ}$C. Solid lines: results of numerical simulation.

eter reported by other researchers [$\nu = 0.40$ (Nitta and Suzuki, 1999), $\nu = 0.42$ (Fellahi et al., 1995), and $\nu = 0.45$ (Lai and Bakker, 1995)]. Poisson's ratio $\nu_2 = 0.490$ is very close to $\nu = 0.5$ for an incompressible medium, which implies that compressibility of HDPE may be neglected in the analysis of its response at tensile strains exceeding 0.015.

3. Model

To study the effect of temperature on mechanical properties of crystalline and amorphous phases separately, we treat HDPE as a

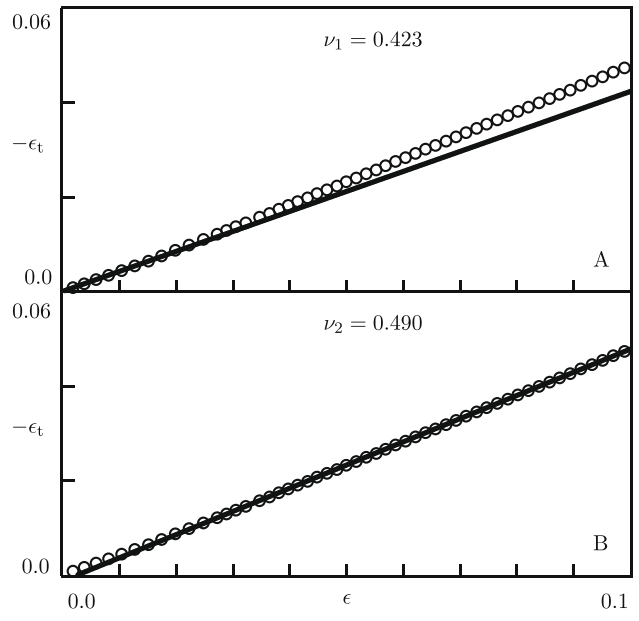

Fig. 6. Transverse strain ϵ_t versus tensile strain ϵ. Circles: experimental data in a tensile test. Solid lines: their approximation by Eq. (1) in the region of linear mechanical response (A) and in the sub-yield region (B).

two-phase composite, where crystalline inclusions are distributed in an amorphous matrix. To reduce the number of adjustable parameters in the stress–strain relations, several hypotheses are introduced regarding the micro-structure of a semicrystalline polymer and its mechanical behavior.

3.1. Basic assumptions

Following common practice (Nikolov and Doghri, 2000; Cangemi and Meimon, 2001; Bedoui et al., 2006; Brusselle-Dupend and Cangemi, 2008), only two phases (amorphous and crystalline) are taken into account. The presence of inter-phases and amorphous regions with reduced molecular mobility located between spherulites and amorphous matrix (Rastogi et al., 2007) or near the fold and stem surfaces (Murthy, 2001) is disregarded.

Both phases are treated as viscoplastic media. Their viscoelastic response associated with rearrangement of chains (Tanaka and Edwards, 1992) in the bulk amorphous phase and cooperative relaxation (Mano, 2001) in crystallites and amorphous domains with restricted molecular mobility is neglected. This assumption appears to be reasonable for the analysis of cyclic tensile tests as the duration of these tests did not exceed 1 min, while our observations in relaxation tests (Drozdov and Christiansen, 2008) show that the decrease in stress during this period was lower than 20% at room temperature, and it does not exceed 10% at temperatures above 45 °C.

To describe the inelastic response of amorphous ($m = 1$) and crystalline ($m = 2$) regions at small deformations, the strain tensor for macro-deformation $\hat{\epsilon}$ is split into the sum of strain tensors for elastic $\hat{\epsilon}_{me}$ and plastic $\hat{\epsilon}_{mp}$ deformations

$$\hat{\epsilon} = \hat{\epsilon}_{me} + \hat{\epsilon}_{mp}. \tag{2}$$

The amorphous phase is modeled as an equivalent non-affine network of chains linked by permanent junctions. Non-affinity means that junctions slide with respect to their reference positions under deformation. The strain rate for plastic deformation in the amorphous phase is proportional to the deviatoric component $\hat{\sigma}'_1$ of an appropriate stress tensor $\hat{\sigma}_1$,

$$\frac{d\hat{\epsilon}_{1p}}{dt} = \Psi_1 \hat{\sigma}'_1, \tag{3}$$

where Ψ_1 is a non-negative function.

The strain tensor for plastic deformation in the crystalline phase equals the sum of two strain tensors associated with intra-crystalline (c-shear) slip (Sirotkin and Brooks, 2001; Guan and Phillips, 2007) and inter-lamellar (sliding of crystalline blocks) flow (Matthews et al., 1999; Jiang et al., 2009)

$$\hat{\epsilon}_{2p} = \hat{e}_{1p} + \hat{e}_{2p}. \tag{4}$$

The strain rate for intra-lamellar deformation is proportional to the deviatoric component $\hat{\sigma}'_2$ of the stress tensor $\hat{\sigma}_2$ in the crystalline phase

$$\frac{d\hat{e}_{1p}}{dt} = \Psi_2 \hat{\sigma}'_2, \tag{5}$$

where Ψ_2 is a non-negative function. The strain rate for inter-lamellar deformation is proportional to the strain rate for macro-deformation

$$\frac{d\hat{e}_{2p}}{dt} = \phi \frac{d\hat{\epsilon}}{dt}. \tag{6}$$

The coefficient ϕ in Eq. (6) satisfies the conditions: (i) ϕ equals zero in the reference state (which means that inter-lamellar slip does not occur at very small deformations), (ii) it monotonically increases with strain (which reflects acceleration of plastic flow under loading), and (iii) it tends to the ultimate value $\phi_\infty = 1$ at large deformations.

3.2. Stress–strain relations

The strain energy density (per unit volume) of a two-phase composite W equals the sum of strain energy densities of amorphous and crystalline phases

$$W = W_1 + W_2. \tag{7}$$

Eq. (7) implies that the energy of interaction between phases in accounted for by means of the incompressibility condition only. The strain energy density of the mth phase $W_m(t)$ $(m = 1, 2)$ is given by the standard relation

$$W_m = \frac{1}{2}\mu_m \hat{\epsilon}_{me} : \hat{\epsilon}_{me}, \tag{8}$$

where μ_m stands for rigidity of the mth phase, and the colon denotes convolution of tensors. The Clausius–Duhem inequality for non-isothermal deformation of an incompressible medium reads

$$Q = T\frac{d\eta}{dt} - \frac{dW}{dt} + \hat{\sigma}' : \frac{d\hat{\epsilon}}{dt} - \frac{1}{T}\bar{q} \cdot \overline{\nabla} T \geqslant 0, \tag{9}$$

where T is absolute temperature, η stands for entropy per unit volume, $\bar{q}$ is the heat flux vector, $\overline{\nabla}$ denotes gradient, Q is the rate of internal entropy production per unit volume, and

$$\hat{\sigma}' = \hat{\sigma}'_1 + \hat{\sigma}'_2 \tag{10}$$

denotes deviator of the stress tensor $\hat{\sigma}$. Inserting Eqs. (7) and (8) into Eq. (9) and using Eqs. (2)–(6), we find that the second law of thermodynamics is satisfied for an arbitrary deformation program, provided that

$$\hat{\sigma}'_1 = \mu_1 \hat{\epsilon}_{1e}, \qquad \hat{\sigma}'_2 = \mu_2(1-\phi)\hat{\epsilon}_{2e}, \tag{11}$$

the specific entropy η is connected with the strain energy density W by the conventional equation

$$\frac{\partial W}{\partial \eta} = T,$$

and the heat flux vector reads

$$\bar{q} = -\kappa \overline{\nabla} T,$$

where κ stands for thermal conductivity. Inequality (9) follows from the formula

$$Q = \Psi_1 \hat{\sigma}'_1 : \hat{\sigma}'_1 + \frac{\Psi_2}{1-\phi}\hat{\sigma}'_2 : \hat{\sigma}'_2 + \frac{\kappa}{T}\overline{\nabla} T \cdot \overline{\nabla} T$$

and the conditions imposed on the functions $\Psi_m(t)$ $(m = 1, 2)$ and $\phi(t)$.

The viscoplastic behavior of a semicrystalline polymer under an arbitrary three-dimensional deformation with small strains is described by

$$\hat{\sigma} = -p\hat{I} + \hat{\sigma}', \tag{12}$$

where p is an unknown pressure, $\hat{I}$ stands for the unit tensor, and $\hat{\sigma}'$ is given by Eqs. (10) and (11).

3.3. Adjustable parameters

Stress–strain relations (10)–(12) together with kinematic equations (2) and (4) and kinetic equations (3) and (5) involve three adjustable functions $\phi(t)$, $\Psi_1(t)$, and $\Psi_2(t)$. To reduce the number of material functions, we set

$$\Psi_m = \frac{\psi \dot{\epsilon}^{eq}}{\mu_m} \qquad (m = 1, 2), \tag{13}$$

where ψ is a non-negative dimensionless function to be determined later, and $\dot{\epsilon}^{eq} = \left(\frac{2}{3}\frac{d\hat{\epsilon}}{dt} : \frac{d\hat{\epsilon}}{dt}\right)^{\frac{1}{2}}$ denotes the equivalent strain rate for macro-deformation.

Evolution of the coefficient ϕ with time is described by the differential equation

$$\frac{d\phi}{dt} = \pm A(1 + be_{2p}^{eq} - \phi)^2, \qquad \phi(0) = 0 \tag{14}$$

with

$$A = a\dot{\epsilon}^{eq}. \tag{15}$$

Here a and b are coefficients that depend on temperature T only, $e_{2p}^{eq} = \left(\frac{2}{3}\hat{e}_{2p} : \hat{e}_{2p}\right)^{\frac{1}{2}}$ stands for the equivalent plastic strain for inter-lamellar shear, and the signs "+" and "−" correspond to loading and unloading, respectively. For uniaxial tension, these processes are determined unambiguously, whereas for an arbitrary three-dimensional deformation, they can be defined following Xia et al. (2005).

When $b = 0$, Eq. (14) is transformed into a conventional second-order kinetic equation, whose order reflects the fact that sliding of crystalline blocks induces sliding of junctions in the amorphous matrix, which, in turn, accelerates plastic flow in the crystalline phase. The second term in parentheses takes into account self-acceleration of inter-lamellar slip driven by plastic deformation of crystallites. The coefficient A in Eq. (14) characterizes duration of a transition regime after which ϕ approaches its ultimate value ϕ_∞. This dimensional parameter is replaced in Eq. (15) with its dimensionless analog a.

The coefficient ψ is independent of strain $\hat{\epsilon}$, but adopts different values under loading and unloading. Its value under loading S_1 is a function of temperature T only: $S_1 = S_1(T)$. Its value under retraction S_2 depends on two parameters: temperature T and equivalent plastic strain $\epsilon_p^{eq} = \left(\frac{2}{3}\hat{\epsilon}_p : \hat{\epsilon}_p\right)^{\frac{1}{2}}$ reached under active loading: $S_2 = S_2(T, \epsilon_p^{eq})$. To distinguish between the effects of temperature and plastic strain tensor (with $\hat{\epsilon}_p = \hat{\epsilon}_{1p} + \hat{\epsilon}_{2p}$), a linear dependence of S_2 on ϵ_p^{eq} is adopted

$$S_2 = s_0 - s_1 \epsilon_p^{eq}, \tag{16}$$

where s_1 is a constant, and $s_0 = s_0(T)$ is a function of temperature.

Given a temperature T and a maximum strain per cycle ϵ_{max}, the mechanical behavior of a semicrystalline polymer under cyclic deformation is determined by six adjustable parameters: μ_1, μ_2, a, b, S_1, and S_2. This number is close to the number of material constants in one-phase constitutive models for cyclic loading, and it is noticeable lower than that in stress–strain relations that account for mechanically induced evolution of microstructure in semicrystalline polymers.

To characterize the effect of temperature on adjustable parameters in the stress–strain relations, the Arrhenius equations are adopted for the coefficient b and the elastic moduli μ_m $(m = 1, 2)$

$$b = b_0 \exp\left(-\frac{H_0}{RT}\right), \qquad \mu_m = \mu_{m0} \exp\left(\frac{H_m}{RT}\right), \tag{17}$$

where b_0 and μ_{m0} stand for pre-factors, H_0 and H_m denote apparent activation energies, and R is the universal gas constant.

The quantities S_1 and s_0, as well as the characteristic strain

$$\epsilon_* = \frac{1}{a} \tag{18}$$

are presumed to linearly depend on temperature T

$$S_1 = S_1^{(0)} + S_1^{(1)} T, \qquad s_0 = s_0^{(0)} + s_0^{(1)} T, \qquad \epsilon_* = \epsilon_*^{(0)} + \epsilon_*^{(1)} T, \tag{19}$$

where $S_1^{(i)}$, $s_0^{(i)}$, and $\epsilon_*^{(i)}$ $(i = 0, 1)$ are constants. Comparison of Eqs. (17) and (19) shows that b and μ_m are treated as parameters strongly (exponentially) affected by temperature, whereas the influence of temperature on other quantities is relatively weak to be approximated by linear functions.

4. Fitting of observations

Adjustable parameters in the stress–strain relations are found by fitting the observations reported in Figs. 1–5. Each set of experimental data is approximated separately.

4.1. Governing equations

It follows from Eqs. (10)–(12) that under uniaxial tensile deformation of an incompressible medium, the engineering stress σ reads

$$\sigma = \sigma_1 + \sigma_2, \qquad \sigma_1 = E_1 \epsilon_{1e}, \qquad \sigma_2 = E_2 (1 - \phi) \epsilon_{2e}, \tag{20}$$

where

$$E_m = \frac{3}{2} \mu_m \qquad (m = 1, 2)$$

stand for appropriate Young's moduli. The elastic strains ϵ_{1e} and ϵ_{2e} are determined from Eqs. (2) and (4)

$$\epsilon_{1e} = \epsilon - \epsilon_{1p}, \qquad \epsilon_{2e} = \epsilon - e_{1p} - e_{2p}, \tag{21}$$

where ϵ stands for tensile strain. Evolution of ϵ_{1p}, e_{1p}, and e_{2p} with ϵ is described by Eqs. (3), (5), (6), and (13)

$$\frac{d\epsilon_{1p}}{d\epsilon} = \frac{\psi}{E_1} \sigma_1, \qquad \frac{de_{1p}}{d\epsilon} = \frac{\psi}{E_2} \sigma_2, \qquad \frac{de_{2p}}{d\epsilon} = \phi, \tag{22}$$

where $\psi = S_1$ at stretching and $\psi = -S_2$ at retraction. Eq. (22) imply that the plastic strains ϵ_{1p} and e_{1p} grow monotonically with time, while e_{2p} increases under tension and decreases under retraction. Changes in the coefficient ϕ are governed by Eqs. (14), (15), and (18)

$$\frac{d\phi}{d\epsilon} = \frac{1}{\epsilon_*} (1 + b e_{2p} - \phi)^2, \tag{23}$$

which provides physical meaning for the characteristic strain ϵ_* as the strain at which plastic flow of junctions in the amorphous matrix reaches it steady state.

4.2. Algorithm of approximation

We begin with matching the stress–strain curves at cyclic loading with the maximum strain $\epsilon_{max} = 0.15$ at various temperatures T. Parameters E_1, E_2, a, b, S_1, and S_2 are calculated by means of the following procedure. First, some intervals $[0, a^\circ]$, $[0, b^\circ]$, $[0, S_1^\circ]$, and $[0, S_2^\circ]$ are fixed, where the best-fit parameters a, b, S_1, and S_2 are located. Each of these intervals is divided into $J = 10$ sub-intervals by the points $a^{(i)} = i\Delta a$, $b^{(j)} = j\Delta b$, $S_1^{(k)} = k\Delta S_1$, and $S_2^{(l)} = l\Delta S_2$ with $\Delta a = a^\circ/J$, $\Delta b = b^\circ/J$, $\Delta S_1 = S_1^\circ/J$, $\Delta S_2 = S_2^\circ/J$, $(i, j, k, l = 0, 1, \ldots, J-1)$. For each set $\left\{a^{(i)}, b^{(j)}, S_1^{(k)}, S_2^{(l)}\right\}$, Eqs. (20)–(23) are integrated the Runge–Kutta method from $\epsilon = 0$ to $\epsilon = \epsilon_{max}$ and from $\epsilon = \epsilon_{max}$ to $\sigma = 0$ with the step $\Delta\epsilon = 1.0 \times 10^{-4}$. The moduli E_1 and E_2 are calculated by the least-squares technique from the condition of minimum of the function

$$F = \sum_m [\sigma^{exp}(\epsilon_m) - \sigma^{num}(\epsilon_m)]^2,$$

where summation is performed over strains ϵ_m at which the observations are reported, σ^{exp} is the engineering stress measured in the test, and σ^{num} is given by Eq. (20). After finding the best-fit values of a, b, S_1, and S_2 from the condition of minimum of F, the initial intervals are replaced with the new intervals $[a - \Delta a, a + \Delta a]$, $[b - \Delta b, b + \Delta b]$, $[S_1 - \Delta S_1, S_1 + \Delta S_1]$, $[S_2 - \Delta S_2, S_2 + \Delta S_2]$, and the calculations are repeated.

When the elastic moduli E_1 and E_2 are determined for each temperature separately, these quantities are plotted versus T in Fig. 7. The data are approximated by Eq. (17)

$$\log E_m = E_m^{(0)} + \frac{E_m^{(1)}}{T} \tag{24}$$

with $\log = \log_{10}$, $E_m^{(0)} = \log\left(\frac{3}{2}\mu_{m0}\right)$, and $E_m^{(1)} = \frac{H_m}{R \ln 10}$. The coefficients $E_m^{(i)}$ $(m = 1, 2; i = 0, 1)$ are found by the least-squares method.

After determination of a, b, and S_1 for each temperature T, the quantity ϵ_* is calculated by means of Eq. (18), and parameters ϵ_*, b, and S_1 are plotted versus T in Figs. 8–10. The data reported in Fig. 8 are matched by Eq. (19), where the coefficients $\epsilon_*^{(0)}$ and $\epsilon_*^{(1)}$ are calculated (by the least-squares technique) in the regions be-

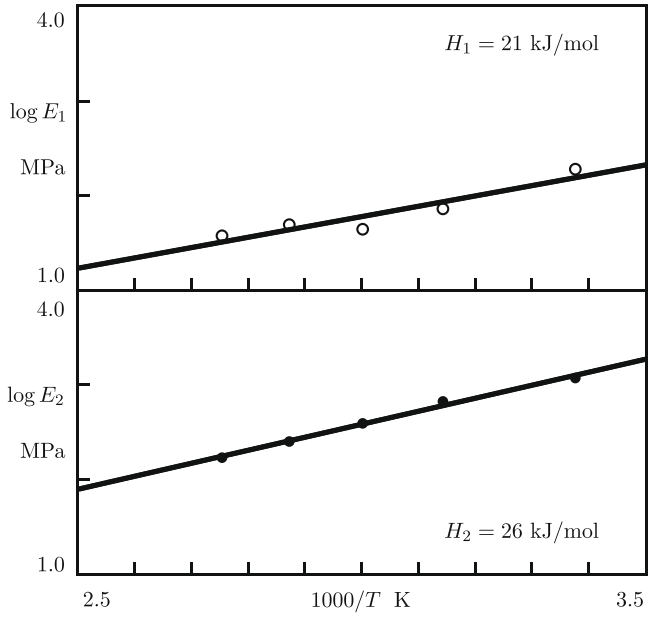

Fig. 7. Elastic moduli E_1 and E_2 versus temperature T. Symbols: treatment of experimental data in cyclic tests. Solid lines: their approximation by Eq. (24).

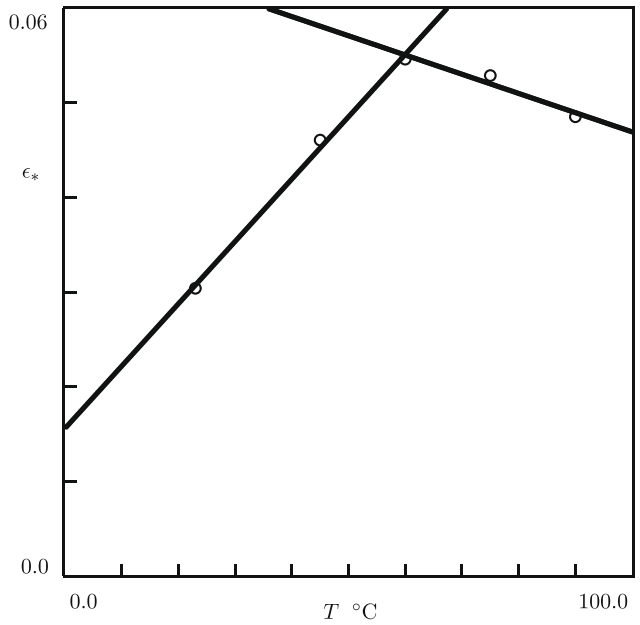

Fig. 8. Characteristic strain ϵ_* versus temperature T. Circles: treatment of experimental data in cyclic tests. Solid lines: their approximation by Eq. (19).

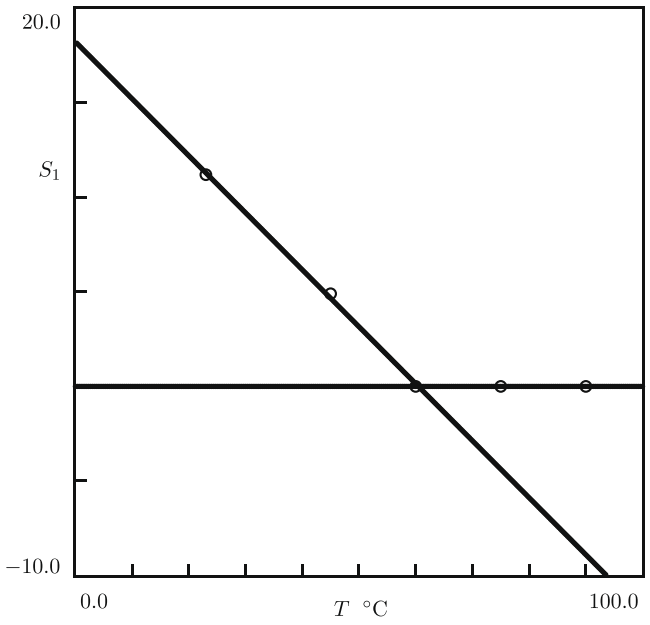

Fig. 10. Dimensionless rate of plastic strain under loading S_1 versus temperature T. Circles: treatment of experimental data in cyclic tests. Solid lines: their approximation by Eq. (19).

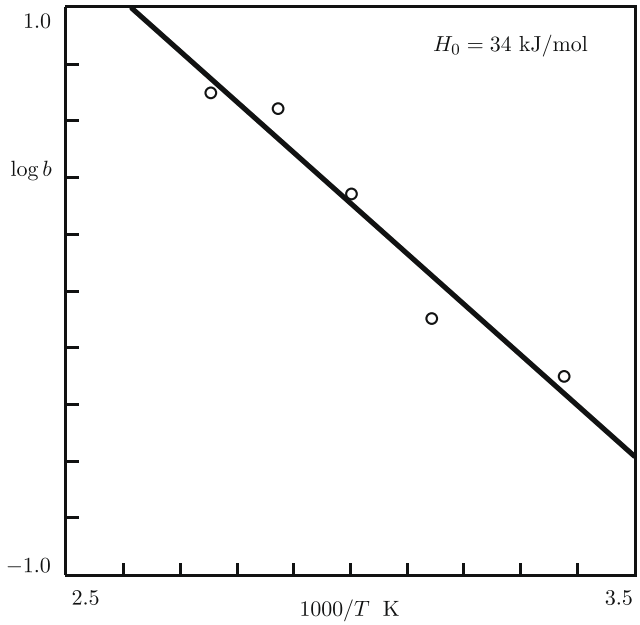

Fig. 9. Dimensionless coefficient b in Eq. (23) versus temperature T. Circles: treatment of experimental data in cyclic tests. Solid line: their approximation by Eq. (25).

low and above T_α separately. Observations presented in Fig. 9 are fitted by Eq. (17)

$$\log b = b^{(0)} - \frac{b^{(1)}}{T} \tag{25}$$

with $b^{(0)} = \log b_0$ and $b^{(1)} = \frac{H_0}{R \ln 10}$. The data depicted in Fig. 10 are approximated by Eq. (19), where the coefficients $S_1^{(0)}$ and $S_1^{(1)}$ are determined by the least-squares method in the intervals $T < T_\alpha$ and $T > T_\alpha$ separately.

We proceed with fitting observations in cyclic tests with $\epsilon_{\max} = 0.05$ and 0.10 at various temperatures T. Given E_1, E_2, a, b, and S_1, each experimental stress–strain curve is determined by the only parameter S_2, which is found by means of the above algorithm.

For each temperature T, the coefficient S_2 is plotted versus maximum plastic strain reached under stretching ϵ_p in Fig. 11. First, the data at $T = 75$ °C are fitted by Eq. (16)

$$S_2 = s_0 - s_1 \epsilon_p, \tag{26}$$

where the coefficients s_0 and s_1 are calculated by means of the least-squares method. Then, the value of s_1 is fixed, and each set of data depicted in Fig. 11 is approximated by Eq. (26) with the only adjustable parameter s_0. When the coefficient s_0 is determined for all temperatures, it is plotted versus T in Fig. 12. The data are matched by Eq. (19), where the coefficients $s_0^{(0)}$ and $s_0^{(1)}$ are calculated in the regions below and above T_α separately.

4.3. Discussion

Figs. 1–5 demonstrate good agreement between the experimental data in tensile cyclic tests with various maximum strains $\epsilon_{\max}$ at various temperatures T and the results of numerical simulation.

Fig. 7 reveals that the Arrhenius equation correctly describes the effect of temperature on Young's moduli of amorphous and crystalline phases. The apparent activation energies H_1 and H_2 adopt similar values (H_2 exceeds H_1 by 26%, but some deviations of experimental data for E_1 from the theoretical dependence should be mentioned). Closeness of H_1 and H_2 is in accord with the results reported by Djokovic et al. (2000) based on treatment of observations in relaxation tests. The activation energies in the range 21–26 kJ/mol are similar to those provided by Zubova et al. (2007) for α-relaxation in HDPE (between 29 and 36 kJ/mol) and Bin Wadud and Baird (2000) for relaxation in polyethylene melts (between 27 and 32 kJ/mol).

Fig. 9 shows that Eq. (17) adequately describes evolution of b with temperature. As H_0 exceeds H_2 by 30% and H_1 by 63%, it is rather difficult to conclude whether thermally induced changes in b, E_1, and E_2 are driven by the same molecular mechanism.

Figs. 8, 10 and 12 demonstrate that slopes of the curves $\epsilon_*(T)$, $S_1(T)$, and $s_0(T)$ alter pronouncedly in the vicinity of

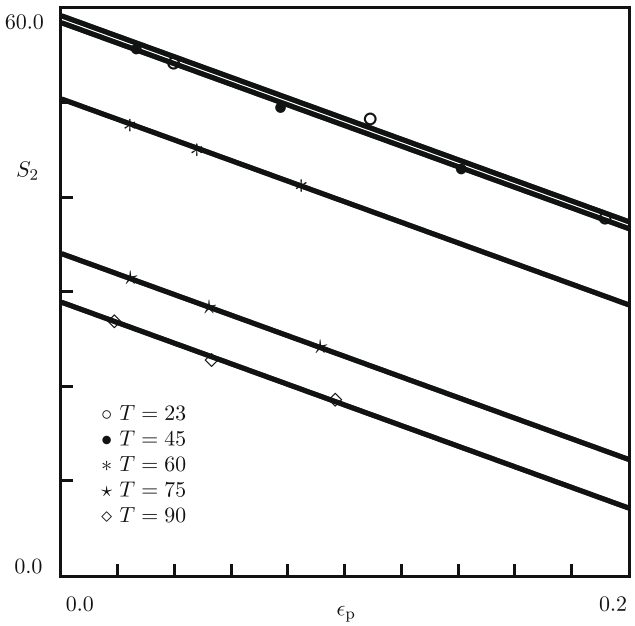

Fig. 11. Dimensionless rate of plastic strain under retraction S_2 versus plastic strain ϵ_p. Symbols: treatment of experimental data in cyclic tests at various temperatures T ° C. Solid lines: their approximation by Eq. (26).

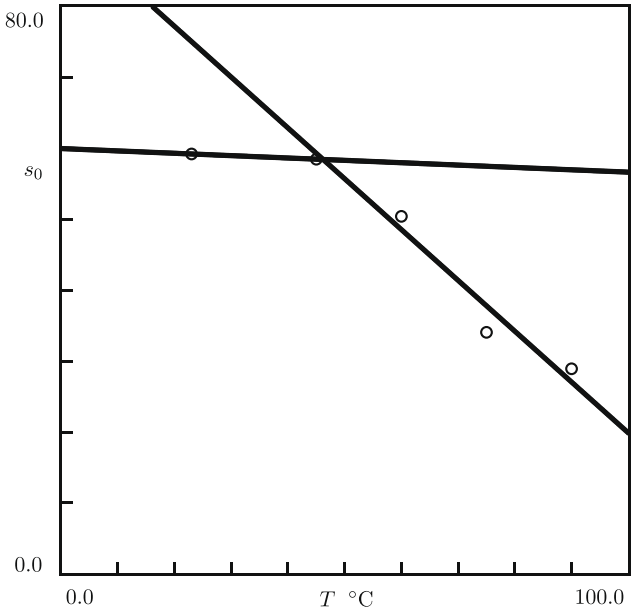

Fig. 12. Strain-independent component of plastic strain rate under retraction s_0 versus temperature T. Circles: treatment of experimental data in cyclic tests. Solid lines: their approximation by Eq. (19).

$T_\alpha \approx 50$—60 °C (this temperature may be identified as the α-relaxation temperature). The value of T_α found in the analysis of observations in cyclic tests is close to the values $T_\alpha = 50$—60 °C (Pegoretti et al., 2000), $T_\alpha = 60$ °C (Drozdov and Christiansen, 2008), $T_\alpha = 70$ °C (Stadler et al., 2005), and $T_\alpha = 50$—70 °C (Na et al., 2007) obtained by using other experimental techniques.

According to Fig. 8, the characteristic strain ϵ_* ranges from 0.03 to 0.06 (depending on temperature). Comparison of these values with appropriate values of the yield strain ϵ_y (Figs. 1–5) implies that developed plastic flow in the amorphous phase is formed in the sub-yield region of deformations, before the tensile stress reaches its maximum.

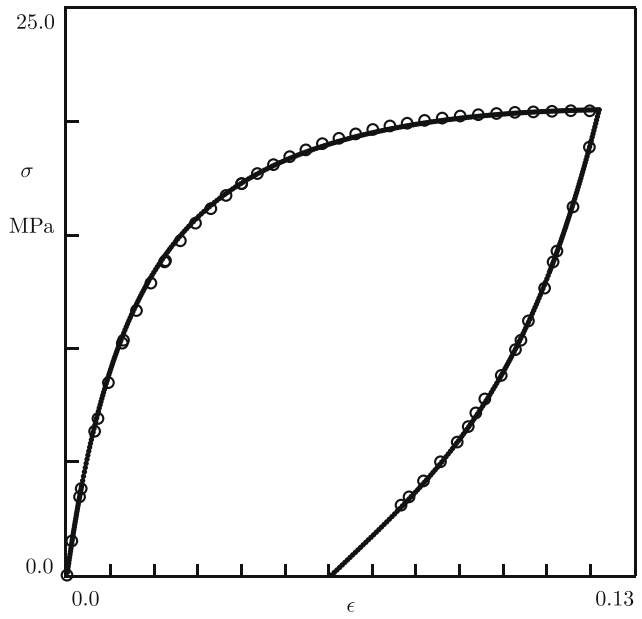

Fig. 13. Stress σ versus strain ϵ. Circles: experimental data in a cyclic test with the maximum strain $\epsilon_{max} = 0.122$ at $T = 23$ ° C. Solid line: prediction of the model.

Fig. 10 together with Eqs. (3) and (5) leads to a rather unexpected conclusion: above the α-relaxation temperature, the coefficient S_1 vanishes. This means that no plastic flow in the amorphous phase and no intra-lamellar slip in the crystalline phase occur under active loading, while inter-lamellar shear provides the only mechanism for inelastic deformation at $T > T_\alpha$. This result, as well as a noticeable decrease in s_0 with T (Fig. 12), appear to be surprising as it is conventionally accepted that the growth of temperature activates all mechanisms for energy dissipation. The above conclusion, however, is in accord with the observations in cyclic tests with $\epsilon_{max} = 0.15$ (Figs. 1–5) which show a pronounced decrease in residual strains with temperature (the latter reflects a reduction of plastic strains acquired under tension and retraction). The decay in plastic flows in amorphous and crystalline domains does not contradict the conventional mechanism of α-relaxation as enhancement of mobility of chains due to release of constraints imposed on their motion at $T < T_\alpha$, but indicates that these constraints play the key role in sliding of junctions in the amorphous matrix and intra-lamellar slip in crystallites.

5. Numerical simulation

Our aim now is to perform numerical simulation of the stress–strain relations in order to (i) validate the model by comparison of observations in independent tests with numerical predictions, and (ii) conduct a thorough analysis of the effects of temperature and maximum strain per cycle on residual strains.

5.1. Validation of the model

To examine the ability of the stress–strain relations to predict the mechanical response of HDPE, two additional cyclic tensile tests were carried out at room temperature with the maximum strains $\epsilon_{max} = 0.12$ and 0.20. In each test, a sample was stretched with the strain rate $\dot\epsilon = 4 \times 10^{-4}$ s^{-1} up to a maximum strain ϵ_{max} and retracted down to the zero stress with the strain rate $-\dot\epsilon$. The experimental data are reported in Figs. 13 and 14 together with the results of numerical simulation. These figures demonstrate that the model correctly predicts the observations.

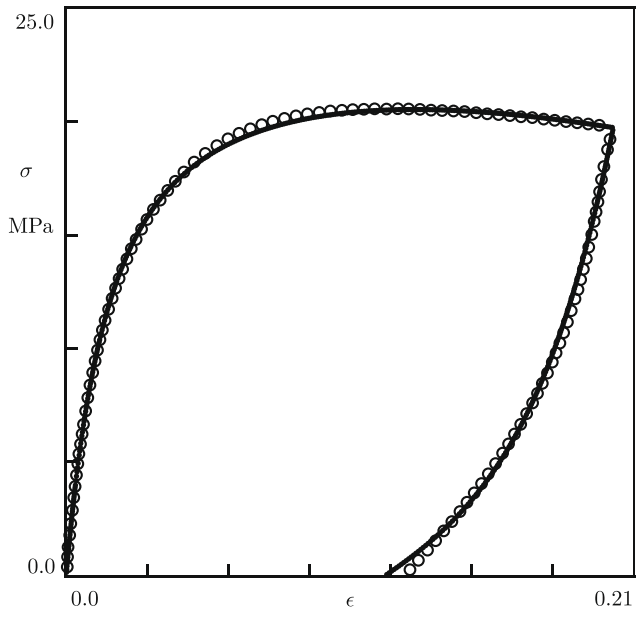

Fig. 14. Stress σ versus strain ϵ. Circles: experimental data in a cyclic test with the maximum strain $\epsilon_{max} = 0.203$ at $T = 23\,^{\circ}$C. Solid line: prediction of the model.

To evaluate the influence of temperature on the viscoplastic behavior of HDPE, numerical analysis is conducted of cyclic tensile tests with the maximum strain $\epsilon_{max} = 0.15$ at $T = 0$, 20, 40, 60, and 80 °C. Appropriate stress–strain diagrams are reported in Fig. 15. To confirm validity of numerical simulation, two tensile cyclic tests were conducted at the temperatures $T = 40$ and 80 °C, and their results are also depicted in Fig. 15. This figure shows (i) a pronounced decrease in the maximum stress (σ_y is reduced by a factor of 4, from 30.4 MPa at $T = 0\,^{\circ}$C to 7.0 MPa at $T = 80\,^{\circ}$C), (ii) a noticeable growth of the yield strain (ϵ_y increases by twice, from 0.060 at $T = 0\,^{\circ}$C to 0.118 at $T = 80\,^{\circ}$C), and (iii) a substantial decay in residual strain (ϵ_{res} decreases by twice, from 0.085 at $T = 0\,^{\circ}$C to 0.045 at $T = 80\,^{\circ}$C). These conclusions are in accord with the experimental data depicted in Figs. 1–5.

5.2. Evolution of residual strains with temperature

To study the effects of temperature and maximum strain on residual strain after a cycle of loading–retraction, numerical simulation is conducted for tensile cyclic tests with $\epsilon_{max} = 0.06$, 0.12, and 0.18 at temperatures T in the interval from 0 to 100 °C. For each ϵ_{max}, the strain ϵ_{res} (reached under unloading down to $\sigma = 0$) is calculated and plotted versus T in Fig. 16. The results of simulation are matched by the linear equation

$$\epsilon_{res} = \epsilon_{res}^{(0)} + \epsilon_{res}^{(1)} T, \tag{27}$$

where the coefficients $\epsilon_{res}^{(0)}$ and $\epsilon_{res}^{(1)}$ are calculated by the least-squares technique in the intervals $T < T_\alpha$ and $T > T_\alpha$ separately.

Fig. 16 shows that (i) for each ϵ_{max}, Eq. (27) correctly approximates results of numerical analysis, (ii) at temperatures below T_α, the residual strain ϵ_{res} is practically independent of temperature when the maximum strain per cycle is below or close to the yield strain, and it weakly decreases with T when ϵ_{max} belongs to the post-yield region of deformations, (iii) at temperatures above the α-relaxation temperature, the residual strain ϵ_{res} strongly decreases with T for all maximum strains ϵ_{max}, (iv) when the maximum strain per cycle lies in the interval of sub-yield deformations, the graph $\epsilon_{res}(T)$ consists of two straight lines that intersect at the α-relaxation temperature, whereas at $\epsilon_{max} > \epsilon_y$, an additional transition region arises near T_α.

6. Concluding remarks

Experimental data are reported on high density polyethylene in tensile loading–unloading tests with a constant strain rate and various maximum strains at temperatures ranging from room temperature to 90 °C (this interval covers the α-relaxation region of HDPE). Observations reveal two characteristic features of the thermo-viscoplastic response: (i) a pronounced reduction in elastic moduli with temperature, and (ii) a decrease in an apparent residual strain (measured at the instant when tensile force vanishes under retraction), which becomes substantial when the maximum strain per cycle exceeds the yield strain.

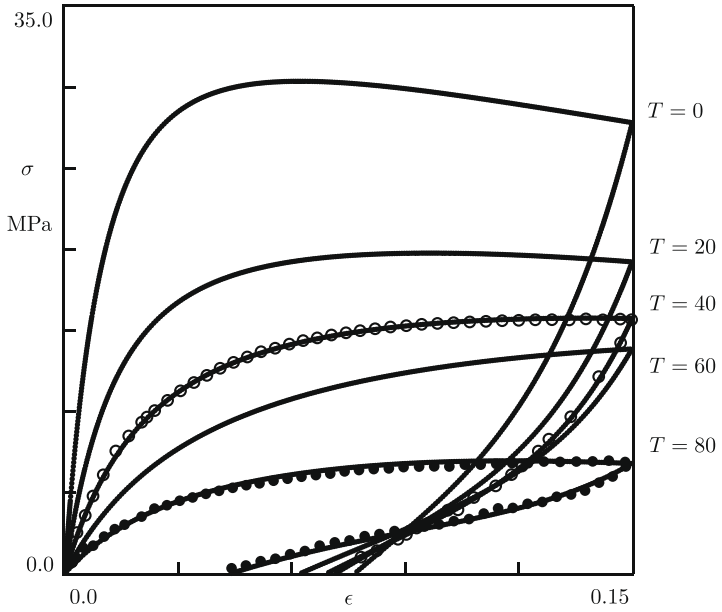

Fig. 15. Stress σ versus strain ϵ. Solid lines: results of numerical simulation for cyclic tests with the maximum strain $\epsilon_{max} = 0.15$ at various temperatures $T\,^{\circ}$C. Symbols: experimental data in cyclic tests at $T = 40\,^{\circ}$C (unfilled circles) and $T = 80\,^{\circ}$C (filled circles).

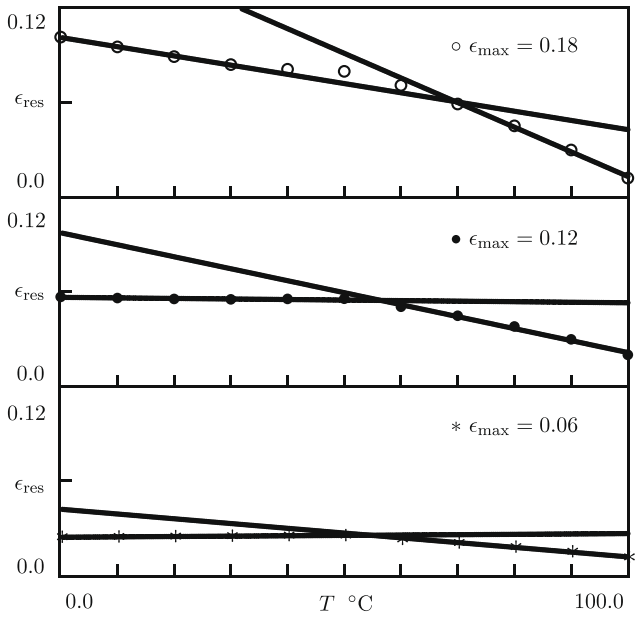

Fig. 16. Residual strain ϵ_{res} versus temperature T. Symbols: results of numerical simulation for cyclic tests with various maximum strains ϵ_{max}. Solid lines: their approximation by Eq. (27).

A model is developed that allows evolution of elastic moduli of amorphous and crystalline phases to be analyzed. A semicrystalline polymer is thought of as a two-phase composite, where crystalline inclusions are distributed in an amorphous matrix. Both phases are treated as viscoplastic media: inelastic deformation in the amorphous phase is attributed to sliding of junctions between chains, whereas plastic flow in spherulites is associated with intra- and inter-lamellar shear. Given a temperature and a maximum strain per cycle, the stress–strain relations involve six adjustable parameters that are found by fitting the observations.

The model adequately describes the experimental data and ensures good accuracy of prediction for observations in independent tests. The latter confirms applicability of the constitutive model with small strains to the analysis of experimental data in tests where the maximum tensile strain does not exceed 20%. Adjustable parameters are affected by temperature in a physically plausible way. In particular, (i) Young's moduli of amorphous and crystalline phases decrease with temperature following the Arrhenius dependencies with similar apparent activation energies, (ii) evolution of ϵ_*, S_1, and S_2 (these quantities characterize the viscoplastic flows in amorphous and crystalline regions) with temperature is fitted by linear equations at low and high temperatures, while the point of intersection of the linear approximations coincides with the α-relaxation temperature. The rates of sliding of junctions in amorphous matrix and intra-lamellar slip in crystallites vanish above T_α, which may serve as a reason for the decay in residual strains observed in cyclic tensile tests.

Acknowledgment

Financial support by the European Commission through project Nanotough-213436 is gratefully acknowledged.

References

Alberola, N., Cavaille, J.Y., Perez, J., 1990. Mechanical spectrometry of alpha relaxations of high-density polyethylene. J. Polym. Sci. B: Polym. Phys. 28, 569–586.

Argon, A.S., 1997. Morphological mechanisms and kinetics of large-strain plastic deformation and evolution of texture in semicrystalline polymers. J. Computer-Aided Mater. Des. 4, 75–98.

Baudet, C., Grandidier, J.-C., Cangemi, L., 2009. A two-phase model for the diffuso-mechanical behaviour of semicrystalline polymers in gaseous environment. Int. J. Solids Struct. 46, 1389–1401.

Bedoui, F., Diani, J., Regnier, G., Seiler, W., 2006. Micromechanical modeling of isotropic elastic behavior of semicrystalline polymers. Acta Mater. 54, 1513–1523.

Ben Hadj Hamouda, H., Laiarinandrasana, L., Piques, R., 2007. Viscoplastic behaviour of a medium density polyethylene (MDPE): constitutive equations based on double nonlinear deformation model. Int. J. Plast. 23, 1307–1327.

Bergstrom, J.S., Kurtz, S.M., Rimnac, C.M., Edidin, A.A., 2002. Constitutive modeling of ultra-high molecular weight polyethylene under large-deformation and cyclic loading conditions. Biomaterials 23, 2329–2343.

Bin Wadud, S.E., Baird, D.G., 2000. Shear and extensional rheology of sparsely branched metallocene-catalyzed polyethylenes. J. Rheol. 44, 1151–1167.

Boyd, R.H., 1979. Modulus of the amorphous component in polyethylenes. Polym. Eng. Sci. 19, 1010–1016.

Boyd, R.H., 1985. Relaxation processes in crystalline polymers: experimental behaviour – a review. Polymer 26, 323–347.

Brusselle-Dupend, N., Cangemi, L., 2008. A two-phase model for the mechanical behaviour of semicrystalline polymers. Part I: large strains multiaxial validation on HDPE. Mech. Mater. 40, 743–760.

Cangemi, L., Meimon, Y., 2001. A two-phase model for the mechanical behavior of semicrystalline polymers. Oil Gas Sci. Technol. 56, 555–580.

Diani, J., Bedoui, F., Regnier, G., 2008. On the relevance of the micromechanics approach for predicting the linear viscoelastic behavior of semi-crystalline poly(ethylene)terephtalates (PET). Mater. Sci. Eng. A 475, 229–234.

Djokovic, V., Kostoski, D., Dramicanin, M.D., 2000. Viscoelastic behavior of semicrystalline polymers at elevated temperatures on the basis of a two-process model for stress relaxation. J. Polym. Sci. B: Polym. Phys. 38, 3239–3246.

Drozdov, A.D., Christiansen, J.deC., 2007a. Cyclic viscoplasticity of high-density polyethylene: experiments and modeling. Comput. Mater. Sci. 39, 465–480.

Drozdov, A.D., Christiansen, J.deC., 2007b. Viscoelasticity and viscoplasticity of semicrystalline polymers: structure–property relations for high-density polyethylene. Comput. Mater. Sci. 39, 729–751.

Drozdov, A.D., Christiansen, J.deC., 2008. Thermo-viscoelastic and viscoplastic behavior of high-density polyethylene. Int. J. Solids Struct. 45, 4274–4288.

Dusunceli, N., Colak, O.U., 2008. Modelling effects of degree of crystallinity on mechanical behavior of semicrystalline polymers. Int. J. Plast. 24, 1224–1242.

Fellahi, S., Favis, B.D., Fisa, B., 1995. Tensile dilatometry of injection-moulded HDPE/PA6 blends. J. Mater. Sci. 30, 5522–5530.

Guan, X., Phillips, P.J., 2007. Dynamic mechanical properties of random ethylene/1-octene copolymers prepared by rapid cooling. Eur. Polym. J. 43, 1219–1233.

Jiang, Z., Tang, Y., Rieger, J., Enderle, H.-F., Lilge, D., Roth, S.V., Gehrke, R., Wu, Z., Li, Z., Men, Y., 2009. Structural evolution of tensile deformed high-density polyethylene at elevated temperatures: Scanning synchrotron small- and wide-angle X-ray scattering studies. Polymer 50, 4101–4111.

Khan, F., Krempl, E., 2006. Amorphous and semicrystalline solid polymers: experimental and modeling studies of their inelastic deformation behaviors. Trans. ASME. J. Eng. Mater. Technol. 128, 64–72.

Khanna, Y.P., Turi, E.A., Taylor, T.J., Vickroy, V.V., Abbott, R.F., 1985. Dynamic mechanical relaxations in polyethylene. Macromolecules 18, 1302–1309.

Kolesov, I.S., Androsch, R., Radusch, H.-J., 2005. Effect of crystal morphology and crystallinity on the mechanical α- and β-relaxation processes of short-chain branched polyethylene. Macromolecules 38, 445–453.

Kuwabara, K., Kaji, H., Horii, F., 2000. Solid-state ^{13}C NMR analyses for the structure and molecular motion in the α relaxation temperature region for metallocene-catalyzed linear low-density polyethylene. Macromolecules 33, 4453–4462.

Lai, J., Bakker, A., 1995. Analysis of the non-linear creep of high-density polyethylene. Polymer 36, 93–99.

Mano, J.F., 2001. Cooperativity in the crystalline α-relaxation of polyethylene. Macromolecules 34, 8825–8828.

Matsuo, M., Bin, Y., Xu, C., Ma, L., Nakaoki, T., Suzuki, T., 2003. Relaxation mechanism in several kinds of polyethylene estimated by dynamic mechanical measurements, positron annihilation, X-ray and ^{13}C solid-state NMR. Polymer 44, 4325–4340.

Matthews, R.G., Unwin, A.P., Ward, I.M., Capaccio, G., 1999. A comparison of the dynamic mechanical relaxation behavior of linear low- and high-density polyethylenes. J. Macromol. Sci. Phys. B 38, 123–143.

Men, Y., Rieger, J., Endeler, H.-F., Lilge, D., 2003. Mechanical α-process in polyethylene. Macromolecules 36, 4689–4691.

Mizuno, M., Sanomura, Y., 2009. Phenomenological formulation of viscoplastic constitutive equation for polyethylene by taking into account strain recovery during unloading. Acta Mech. 207, 83–93.

Murthy, N.S., 2001. Glass transition temperature and the nature of the amorphous phase in semicrystalline polymers: Effects of drawing, annealing and hydration in polyamide 6. Int. J. Polym. Mater. 50, 429–444.

Na, B., Lv, R., Xu, W., Yu, P., Wang, K., Fu, Q., 2007. Inverse temperature dependence of strain hardening in ultrahigh molecular weight polyethylene: Role of lamellar coupling and entanglement density. J. Phys. Chem. B 111, 13206–13210.

Nikolov, S., Doghri, I., 2000. A micro/macro-constitutive model for the small-deformation behavior of polyethylene. Polymer 41, 1883–1891.
Nikolov, S., Lebensohn, R.A., Raabe, D., 2006. Self-consistent modeling of large plastic deformation, texture and morphology evolution in semi-crystalline polymers. J. Mech. Phys. Solids 54, 1350–1375.
Nitta, K.-H., Suzuki, K., 1999. Prediction of stress-relaxation behavior in high density polyethylene solids. Macromol. Theory Simul. 8, 254–259.
Olasz, L., Gudmundson, P., 2005. Prediction of residual stresses in cross-linked polyethylene cable insulation. Polym. Eng. Sci. 45, 1132–1139.
Pegoretti, A., Ashkar, M., Migliaresi, C., Marom, G., 2000. Relaxation processes in polyethylene fibre-reinforced polyethylene composites. Compos. Sci. Technol. 60, 1181–1189.
Popli, R., Mandelkern, L., Benson, R.S., 1984. Dynamic mechanical studies of α- and β-relaxations in polyethylenes. J. Polym. Sci. B: Polym. Phys. 22, 407–448.
Rastogi, S., Lippits, D.R., Terry, A.E., Lemstra, P.J., 2007. The role of the interphase on the chain mobility and melting of semi-crystalline polymers: a study on polyethylenes. Lect. Notes Phys. 714, 285–327.
Regrain, C., Laiarinandrasana, L., Toillon, S., Sai, K., 2009. Multi-mechanism models for semi-crystalline polymer: constitutive relations and finite element implementation. Int. J. Plast. 25, 1253–1279.
Roguet, E., Castagnet, S., Grandidier, J.C., 2007. Mechanical features of the rubbery amorphous phase in tension and torsion in a semi-crystalline polymer. Mech. Mater. 39, 380–391.
Sirotkin, R.O., Brooks, N.W., 2001. The dynamic mechanical relaxation behaviour of polyethylene copolymers cast from solution. Polymer 42, 9801–9808.
Stadler, F.J., Kaschta, J., Munstedt, H., 2005. Dynamic-mechanical behavior of polyethylenes and ethene-/α-olefin-copolymers Part I. α'-relaxation. Polymer 46, 10311–10320.
Sweeney, J., Naz, S., Coates, P.D., 2009. Viscoplastic constitutive modeling of polymers – flow rules and the plane strain response. J. Appl. Polym. Sci. 111, 1190–1198.
Tanaka, F., Edwards, S.F., 1992. Viscoelastic properties of physically cross-linked networks. Transient network theory. Macromolecules 25, 1516–1523.
van Dommelen, J.A.W., Parks, D.M., Boyce, M.C., Brekelmans, W.A.M., Baaijens, F.P.T., 2003. Micromechanical modeling of the elasto-viscoplastic behavior of semi-crystalline polymers. J. Mech. Phys. Solids 51, 519–541.
van Dommelen, J.A.W., Brekelmans, W.A.M., Govaert, L.E., 2007. Multiscale modelling of the mechanical behaviour of oriented semicrystalline polymers. Mater. Sci. Forum 539–543, 2607–2612.
Xia, Z., Shen, X., Ellyin, F., 2005. An assessment of nonlinearly viscoelastic constitutive models for cyclic loading: the effect of a general loading/unloading rule. Mech. Time-Dependent Mater. 9, 281–300.
Yakimets, I., Lai, D., Guigon, M., 2007. Model to predict the viscoelastic response of a semi-crystalline polymer under complex cyclic mechanical loading and unloading conditions. Mech. Time-Dependent Mater. 11, 47–60.
Zubova, E.A., Balabaev, N.K., Manevitch, L.I., 2007. Molecular mechanisms of the chain diffusion between crystalline and amorphous fractions in polyethylene. Polymer 48, 1802–1813.